



Structural and catalytic properties of supported Ni–Ir alloy catalysts for H₂ generation via hydrous hydrazine decomposition

Lei He ^{a,b}, Yanqiang Huang ^{a,*}, Xiao Yan Liu ^a, Lin Li ^a, Aiqin Wang ^a, Xiaodong Wang ^a, Chung-Yuan Mou ^c, Tao Zhang ^{a,*}

^a State Key Laboratory of Catalysis, Dalian Institute of Chemical Physics, Chinese Academy of Sciences, 457 Zhongshan Road, Dalian 116023, China

^b University of Chinese Academy of Sciences, 19A Yuquan Road, Beijing 100049, China

^c Department of Chemistry, National Taiwan University, Taipei 10617, Taiwan



ARTICLE INFO

Article history:

Received 19 August 2013

Received in revised form

13 September 2013

Accepted 10 October 2013

Available online 17 October 2013

Keywords:

Nickel–iridium alloy

Hydrazine

Hydrogen storage

EXAFS

Microcalorimeter

ABSTRACT

Iridium modified Ni/Al₂O₃ catalysts were prepared using Ni–Al hydroxide as precursor and tested in the selective decomposition of hydrous hydrazine for H₂ generation. Compared to Ni/Al₂O₃, NiIr_x/Al₂O₃ catalysts exhibited an increase of the reaction rate up to 6-fold and the H₂ selectivity from 93% to above 99%. The XRD and EXAFS analysis confirmed that Ir and Ni were present in the form of Ni–Ir alloy; and the H₂ differential heat of adsorption is appreciably lowered with increasing the amount of Ir in Ni–Ir alloy. High-temperature reduction, e.g. 700 °C, induced the migration of Ir atoms into the Ni bulk and produced a Ni-skin surface. This structural modification is associated with a strongly decrease of activity and selectivity. EXAFS measurements were also performed on different noble metals (NM, Ir, Pt, and Au) modified Ni/Al₂O₃ catalysts in order to verify the extent of NM–Ni bimetallic bond formation, which was found to correlate with the catalytic performance.

© 2013 Elsevier B.V. All rights reserved.

1. Introduction

Chemical hydrogen storage material is a promising candidate of hydrogen storage with the advantages of its considerable hydrogen content and convenient transformation [1]. Among the variety of liquid hydrogen storage materials, hydrous hydrazine, such as hydrazine monohydrate (N₂H₄·H₂O) with a high content of hydrogen (8.0 wt%), has been discovered as a hydrogen source for its unique advantage that N₂ is the only by-product for the complete decomposition (H₂NNH₂ → N₂(g) + 2H₂(g)) [2–4]. However, it is undesirable for the occurrence of incomplete decomposition (3H₂NNH₂ → 4NH₃(g) + N₂(g)), through which no hydrogen could be released [5,6]. Moreover, the existence of by-product NH₃ could also complicate the separation process and may poison the Nafion membrane and fuel-cell catalysts. Therefore, it is of great importance to develop effective catalysts for selective decomposition of hydrous hydrazine to hydrogen at mild conditions.

Many different catalytic systems have been developed to achieve the goal of selective decomposition of hydrous hydrazine, such as bimetallic nanoparticles [7–10], composite oxides [11,12], supported nanocatalysts [13–18], and so on. Among them, Ni-based

bimetallic catalysts are the most efficient ones for this reaction. Xu and coworkers firstly synthesized various bimetallic nanoparticles. Especially, the combination of Rh, Pt, and Ir to Ni could catalyze the complete decomposition of hydrous hydrazine at room temperature with 100% H₂ selectivity [7–9]. In addition, they found that Ni–Fe nanoparticles could also catalyze this reaction at 70 °C with the assistance of NaOH [10]. However, the nanoparticles showed poor kinetic and were often difficult to separate because of the usage of surfactants. In this case, supported metallic nanocatalysts are preferred for their advantages of high metal dispersion, good mechanical stability, and easy separation from the reaction medium. Zhang's group [13] prepared graphene supported Rh–Ni catalyst, with the promotion effect of NaOH, which exhibited 100% selectivity to H₂ and a much higher catalytic efficiency compared with bare Rh–Ni nanoparticles. Meanwhile, He et al. [16] synthesized monometallic Ni/Al₂O₃ catalyst derived from Ni–Al hydroxide precursor, which catalyzed the reaction with 93% H₂ selectivity. On the basis of this work, bimetallic NiPt_x/Al₂O₃ catalysts were prepared by doping little amount of Pt to Ni–Al hydroxide, which significantly promoted the reaction rate and the H₂ selectivity to over 98% [17]. Recently, Tong et al. [18] synthesized monodispersed Ni₃Fe nanospheres supported on carbon, which also showed an excellent performance for this reaction. Although the experiments have proved that supported Ni-based bimetallic catalysts exhibited desired performance for this reaction, the detailed structure of the catalysts and the surface adsorption

* Corresponding authors. Tel.: +86 411 84379416; fax: +86 411 84685940.

E-mail addresses: yqhuang@dicp.ac.cn (Y. Huang), [\(T. Zhang\)](mailto:taozhang@dicp.ac.cn).

properties remain to be investigated to reveal the inner reason for their desired selectivity and activity.

Ir/Al₂O₃ is the most reactive catalyst for hydrazine decomposition. But its H₂ selectivity was only ~6% at ambient temperature because of the easier N–N bond cleavage in hydrazine than that of N–H bond [8,19]. As mentioned above, Ni/Al₂O₃ catalyst derived from Ni–Al hydrotalcite showed a high H₂ selectivity (~93%) at 30 °C, but its reactivity remains to be promoted. In this paper, supported NiIr_x/Al₂O₃ catalysts were prepared by doping different amounts of Ir on Ni–Al hydrotalcite. The reactivity performance and the detailed structure were studied for all the catalysts. Microcalorimetry experiments were also carried out to investigate the H₂ adsorption property over different Ni–Ir bimetallic catalysts. To further investigate the role of additional Ir, NiIr_{0.059}/Al₂O₃ catalyst was pre-reduced in different temperatures to obtain samples with different structural configurations. The structure and reactivity changes were fully investigated and these results could provide evidences for the reason of good performance of Ni–Ir bimetallic catalysts. Furthermore, different noble metals doped Ni catalysts (Ni–Ir, Ni–Pt, and Ni–Au) were also compared to examine the model we built.

2. Experimental

2.1. 2.1 Catalyst preparation

Ni–Al hydrotalcite was prepared using co-precipitant (CP) method as the precursor for monometallic Ni/Al₂O₃ and bimetallic NiIr_x/Al₂O₃ catalysts ($x = 0.016, 0.030, 0.046$ and 0.059 , molar ratio between Ir and Ni) [16,17,20]. The monometallic Ni/Al₂O₃ catalyst was obtained by reducing the Ni–Al hydrotalcite directly at 500 °C in pure hydrogen [16]. For the preparation of NiIr_x/Al₂O₃ catalysts, deposition–precipitation (DP) method was employed using urea as the precipitant [17]. Briefly, Ni–Al hydrotalcite precursor (1.00 g) was previously dispersed into deionized water (150 mL) with the assistance of ultrasonic. Then prescribed amount of H₂IrCl₆ solution (containing 20–80 mg Ir) was added dropwise into the suspension under magnetic stirring. Proper amount of urea (10-folds of necessarily amount of OH[−]) was added simultaneously. Afterwards, the temperature was increased to 90 °C and kept for 8 h under continuously stirring. The as-prepared deposit was filtered, washed with water for 5 times, dried at 80 °C and then reduced in pure hydrogen at 300 °C for 1 h to get NiIr_x/Al₂O₃ catalysts. To be noted, all of the freshly reduced catalysts were protected in deaerated water before hydrous hydrazine decomposition test in order to avoid oxidation.

To investigate the structural changes under different reduction temperatures, NiIr_{0.059}/Al₂O₃ catalyst was further pretreated at 500 °C and 700 °C in pure H₂, respectively. The obtained catalysts were denoted as NiIr_{0.059}/Al₂O₃-500R and NiIr_{0.059}/Al₂O₃-700R.

For comparison with NiIr_{0.030}/Al₂O₃ catalyst, bimetallic NiPt/Al₂O₃ and NiAu/Al₂O₃ catalysts were also prepared by DP method described above, using H₂PtCl₆ and H₂AuCl₄ as precursor containing the same weight of noble metal as Ir for NiIr_{0.030}/Al₂O₃. The actual loading of Au and Pt were determined by ICP analysis. Before the reaction test, NiIr_{0.030}/Al₂O₃ and NiPt_{0.027}/Al₂O₃ samples were reduced at 300 °C, while NiAu_{0.020}/Al₂O₃ was reduced at 350 °C (according to the H₂-TPR results). In addition, monometallic Ir/Al₂O₃, Pt/Al₂O₃, and Au/Al₂O₃ catalysts were also prepared through the same procedure using γ-Al₂O₃ ($S_{BET} = 243.5 \text{ m}^2 \text{ g}^{-1}$) as the support.

2.2. Hydrous hydrazine decomposition test

The test was carried out in a three-necked round bottom flask, of which one neck was connected to an air-tight gas burette for

Table 1
Catalyst composition determined by inductively coupled plasma (ICP) spectrophotometry.

Catalysts	Ir (wt%)	Ni (wt%)	Al (wt%)	Ir/Ni (molar ratio)
Ni/Al ₂ O ₃	0	38.3	6.0	0
NiIr _{0.016} /Al ₂ O ₃	2.0	36.8	6.1	0.016
NiIr _{0.030} /Al ₂ O ₃	3.7	36.2	5.8	0.030
NiIr _{0.046} /Al ₂ O ₃	5.7	37.2	5.8	0.046
NiIr _{0.059} /Al ₂ O ₃	6.7	34.3	5.5	0.059

volume calculation [16,17]. The reaction temperature was controlled by water bath. Before the decomposition test, ~40.0 mg of catalyst (the precursor was 90.0 mg before reduction) was previously put into the reactor. The reaction was initiated by injecting 5.0 mL N₂H₄·H₂O solution (0.32 mol L^{−1}) into the reactor under magnetic stirring. Reaction rate (h^{−1}) for different catalysts was calculated by assuming that all the metal atoms took part in the reaction with 50% conversion of hydrous hydrazine as described by Xu [9].

The selectivity to H₂(x) is calculated on the basis of the following equation: $3 \text{N}_2\text{H}_4 \rightarrow 4(1-x) \text{NH}_3 + 6x \text{H}_2 + (1+2x) \text{N}_2$. The gas volume measured at the end of the reaction containing only N₂ and H₂, from which the molar ratio of $n(\text{N}_2 + \text{H}_2)/n(\text{N}_2\text{H}_4)$ (λ) was obtained. Therefore, the selectivity could be calculated as follows [17]:

$$x = \frac{3\lambda - 1}{8} \quad \left[\lambda = \frac{n(\text{N}_2 + \text{H}_2)}{n(\text{N}_2\text{H}_4)} \left(\frac{1}{3} \leq \lambda \leq 3 \right) \right]$$

For the stability test of NiIr_{0.059}/Al₂O₃ catalyst, the decomposition reaction was carried out over the same catalyst for 10 cycles. The catalyst was separated by a magnet after each cycle and reused.

2.3. Catalyst characterization

Chemical compositions of all the catalysts were determined by using Thermo IRIS Intrepid II inductively coupled plasma (ICP). The exact contents of Ir, Ni, and Al in the catalysts were listed in Table 1.

Micromeritics AutoChem II 2920 Automated Catalyst Characterization System was employed for temperature-programmed reduction (TPR) experiments. Before the experiment, ~30 mg of un-reduced sample was loaded into a U-shape quartz reactor and pretreated with Ar at 150 °C for 1 h to remove adsorbed water. After cooling to 50 °C, the flowing gas was switched to 10 vol% H₂/Ar. When the baseline was stable, the sample was heated to 900 °C at a ramping rate of 10 °C min^{−1}. The amount of H₂ consumption during reduction was monitored by a thermal conductivity detector (TCD). A cold trap filled with a mixture of isopropanol and liquid nitrogen was placed between the sample and the TCD to remove generated water.

X-ray diffraction (XRD) tests were performed on a PANalytical X'Pert-Pro powder X-ray diffractometer, using nickel-filtered Cu K_α monochromatized radiation ($\lambda = 0.1541 \text{ nm}$) with a scanning angle (2θ) of 10–80° at a scan speed of 6° min^{−1}, operated at 40 kV and 40 mA. All of the freshly reduced catalysts were protected in Ar to avoid oxidation.

HAADF-STEM images were recorded on a Tecnai G220 S-Twin microscopy. The reduced catalysts were suspended on a copper grid before the analysis.

The X-ray absorption fine structure (XAFS) spectra of Ir L₃-edge were measured at the BL-9C station of the Photon Factory at the BL14W1 beamline of the Shanghai Synchrotron Radiation Facility (SSRF). X-ray absorption near edge structure (XANES) and extended X-ray absorption fine structure (EXAFS) spectra were recorded at room temperature in fluorescence mode for all the Ir-doped catalysts as well as Ir foil and IrO₂ standard samples. The NiIr_x/Al₂O₃ catalysts were firstly reduced at 300 °C as for the

decomposition tests and protected under inert atmosphere to prevent oxidation. For comparison, the Ir L₃-edge spectra were also taken for NiIr_{0.059}/Al₂O₃ pre-reduced at different temperatures. Besides, Pt L₃-edge spectra for NiPt_{0.027}/Al₂O₃ and Au L₃-edge spectra for NiAu_{0.020}/Al₂O₃ catalysts were also obtained using the same beamline. The XAFS data analyzing and fitting were carried out by using IFFEFIT 1.2.11 data analysis package (Athena, Artemis, Atoms, and FEFF6). The raw data were reduced by aligning the scans to the foil standard and deglitching when necessary to reduce experimental error. By using AUTOBK algorithm in Athena, the isolated-atom background function was removed from the XAFS data. And then the treated data were Fourier transformed into R-space for further fitting. Local structural information was obtained using Artemis to fit each data set with theoretical standards generated by FEFF6 in R-space. The theoretical Ir–Ir photoelectron amplitudes and phases were calculated for the bulk Ir fcc structure. Ni–Ir contributions were calculated by replacing Ir with Ni in the first nearest-neighbor shell. The same calculation was used for Ni–Pt and Ni–Au catalysts.

Microcalorimetric tests of H₂ adsorption were performed using a BT 2.15 heat-flux calorimeter at 40 °C. The calorimeter was connected to a gas handling equipment and a volumetric system employing MKS 698A Baratron Capacitance Manometers for precision pressure measurement ($\pm 1.33 \times 10^{-2}$ Pa). The maximum apparent leak rate of the volumetric system was 10^{-4} Pa min⁻¹ in a system volume of approximately 80 cm³. The ultimate dynamic vacuum of the system was ca. 10^{-5} Pa. The samples were pre-reduced in pure hydrogen and then protected in He before the test.

3. Results and discussion

3.1. NiIr_x/Al₂O₃ catalysts for the selective decomposition of hydrous hydrazine

3.1.1. Hydrous hydrazine decomposition test

The catalytic performances of Ir/Al₂O₃, Ni/Al₂O₃, and NiIr_x/Al₂O₃ catalysts were compared in hydrous hydrazine decomposition test at 30 °C (Fig. 1). As listed in Table 2, Ni/Al₂O₃ catalyst exhibited a high H₂ selectivity (93%) but the lowest reaction rate (2.2 h⁻¹), while Ir/Al₂O₃ showed the highest reaction rate (788.0 h⁻¹) but poor selectivity (only 6%). In comparison with the parent monometallic Ni catalysts, NiIr_x/Al₂O₃ catalysts exhibited an enhanced catalytic performance with both higher activity and

Table 2

Comparison of selectivity and activity for hydrous hydrazine decomposition tests over NiIr_x/Al₂O₃ catalysts at 30 °C.

Catalysts	Ni particle size (nm)	Selectivity x (%)	Reaction rate ^a (h ⁻¹)
Ni/Al ₂ O ₃	4.0	93	2.2
Ir/Al ₂ O ₃	1.4 ^b	6	788.0
NiIr _{0.016} /Al ₂ O ₃	3.0	99	6.3
NiIr _{0.030} /Al ₂ O ₃	3.0	99	8.0
NiIr _{0.046} /Al ₂ O ₃	3.0	98	12.0
NiIr _{0.059} /Al ₂ O ₃	3.0	99	12.4
NiIr _{0.059} /Al ₂ O ₃ –10th cycle	3.0	98	9.2

^a The reaction rate were calculated when the conversion was 50%.

^b It was calculated from HRTEM image of Ir/Al₂O₃.

selectivity for hydrogen generation. Upon addition only 0.016 (molar ratio to Ni) of Ir, the selectivity to H₂ increased to 99% with the reaction rate of 6.3 h⁻¹ (Table 2). As the amount of additional Ir increased to 0.030, 0.046, and 0.059, the corresponding reaction rate increased to 8.0 h⁻¹, 12.0 h⁻¹, and 12.4 h⁻¹, respectively. Meanwhile, the selectivity to H₂ remained higher than 98% on all three samples.

In addition to the desired H₂ selectivity and activity of Ir-modified catalysts, further investigation was carried out to check the stability of NiIr_{0.059}/Al₂O₃ catalyst. We took 10 cycles of reactions over the same catalyst at 30 °C by using a magnet to collect the catalyst after each cycle and reuse it again. As shown in Fig. S1 (supporting information), the H₂ selectivity remained as high as 98% with no decline after recycling, but the reaction rate slightly decreased after each cycle. After 10 cycles of reaction, the reaction rate decreased to 9.2 h⁻¹, but still much higher than Ni/Al₂O₃ catalyst. Furthermore, the apparent active energies (E_a) were calculated from the slopes of the linear curves for hydrous hydrazine decomposition over Ni/Al₂O₃ and NiIr_{0.059}/Al₂O₃ catalysts (Fig. 2). Compared with the E_a over Ni/Al₂O₃ (49.3 kJ mol⁻¹), the value over NiIr_{0.059}/Al₂O₃ was lower (38.6 kJ mol⁻¹), similar to that observed on Ni–Pt catalyst [17]. To be noted, the H₂ selectivity remained higher than 98% when the reaction temperature increased from 30 °C to 80 °C over NiIr_{0.059}/Al₂O₃ (Table 3). This is quite different from that observed on Ni/Al₂O₃, which exhibited a decrease of H₂ selectivity to 82% at 80 °C. This sustainable high selectivity over a wider range of temperature will be beneficial in application since this is an exothermic reaction [4]. Obviously, the additional Ir plays a positive role in promoting catalytic performance of Ni-based catalyst.

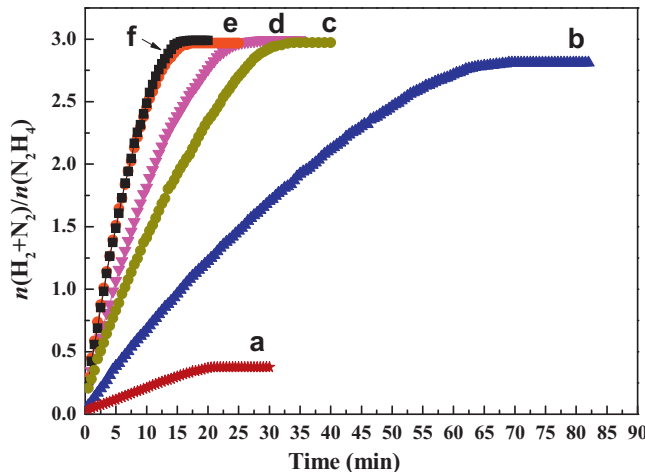


Fig. 1. Time profiles for the hydrous hydrazine decomposition tests at 30 °C over: (a) Ir/Al₂O₃ catalyst; (b) Ni/Al₂O₃ catalyst; (c) NiIr_{0.016}/Al₂O₃ catalyst; (d) NiIr_{0.030}/Al₂O₃ catalyst; (e) NiIr_{0.046}/Al₂O₃ catalyst; (f) NiIr_{0.059}/Al₂O₃ catalyst. The Ir loading in Ir/Al₂O₃ catalyst was the same as in NiIr_{0.016}/Al₂O₃ catalyst.

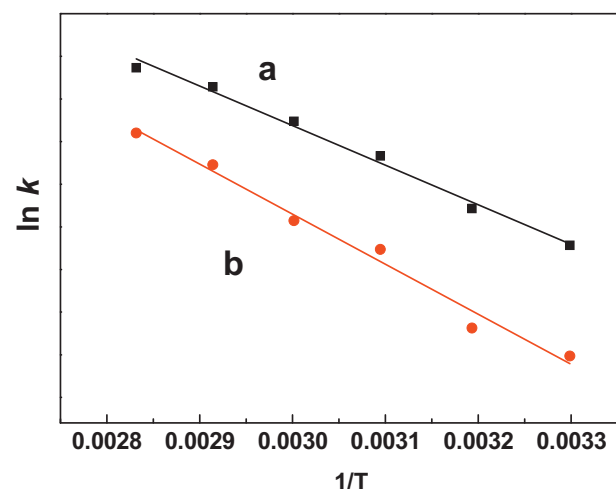


Fig. 2. The comparison of Arrhenius plots for: (a) NiIr_{0.059}/Al₂O₃ catalyst; (b) Ni/Al₂O₃ catalyst.

Table 3

Comparison of hydrous hydrazine decomposition tests over $\text{NiIr}_{0.059}/\text{Al}_2\text{O}_3$ and $\text{Ni}/\text{Al}_2\text{O}_3$ catalysts at different reaction temperatures.

Reaction temperature (°C)	$\text{NiIr}_{0.059}/\text{Al}_2\text{O}_3$		$\text{Ni}/\text{Al}_2\text{O}_3$	
	Reaction rate (h ⁻¹)	Selectivity (%)	Reaction rate (h ⁻¹)	Selectivity (%)
30	12.4	>99	2.2	93
40	19.7	>99	2.8	93
50	36.9	99	7.8	93
60	55.9	98	11.6	91
70	84.3	97	23.3	87
80	105.7	97	34.6	82

3.1.2. Structural analysis of $\text{NiIr}_x/\text{Al}_2\text{O}_3$ catalysts

Fig. 3 presents H₂-TPR profiles of the Ni-Al hydrotalcite together with the fresh Ir modified samples. For $\text{Ni}/\text{Al}_2\text{O}_3$ catalyst, the hydrogen consumption peak was centered at 490 °C, which represented the reduction of Ni^{2+} . Two invert peaks at 200 °C and 315 °C were corresponded to the formation of H_2O and CO_2 , originated from the decomposition of NiAl-HT precursor. For $\text{NiIr}_x/\text{Al}_2\text{O}_3$ catalysts, the main hydrogen consumption peak for each catalyst was one single peak below 300 °C, much lower than that for $\text{Ni}/\text{Al}_2\text{O}_3$ catalyst, indicating that the addition of Ir significantly promoted reduction of Ni, as has been noted previously [21,22]. The reason for this promotion was that the H₂ spillover effect occurred over noble metals. It is easier for H₂ dissociation on Ir, followed by spillover of atomic H to Ni next to it. Therefore, this spillover effect leads to the simultaneous reduction of Ni and Ir at lower temperatures. We chose the reduction temperatures for different catalysts on the basis of H₂-TPR results.

XRD results of $\text{Ni}/\text{Al}_2\text{O}_3$ and $\text{NiIr}_x/\text{Al}_2\text{O}_3$ catalysts are compared in Fig. 4. For $\text{Ni}/\text{Al}_2\text{O}_3$ catalyst (Fig. 4a), three main diffraction peaks could be observed with 2θ values of 44.4°, 51.7°, and 76.3°, belonging to (111), (200), and (220) planes of metallic Ni (PDF no. 01-087-0712), respectively. For all $\text{NiIr}_x/\text{Al}_2\text{O}_3$ catalysts, there is neither IrO_2 nor metallic Ir diffraction peak observed in the XRD patterns (Fig. 4b–e), indicating that Ir species are highly dispersed among the catalysts with very small particle size which could not be detected by XRD. Meanwhile, after the addition of Ir, the 2θ values for main diffraction peaks were 44.0°, 51.4°, and 75.9°, which were slightly shifted to lower angles compared with the peaks of Ni. This little shift is probably due to the alloying of Ir with Ni, as Ir has larger atomic diameter than Ni. According to Bragg's equation, the expansion of lattice parameter causes the shift of diffraction peak to lower angles [23]. The XRD patterns give a brief understanding that Ni–Ir alloy was formed during the reduction pretreatment of Ir-doped catalysts. All the $\text{NiIr}_x/\text{Al}_2\text{O}_3$ catalysts with different

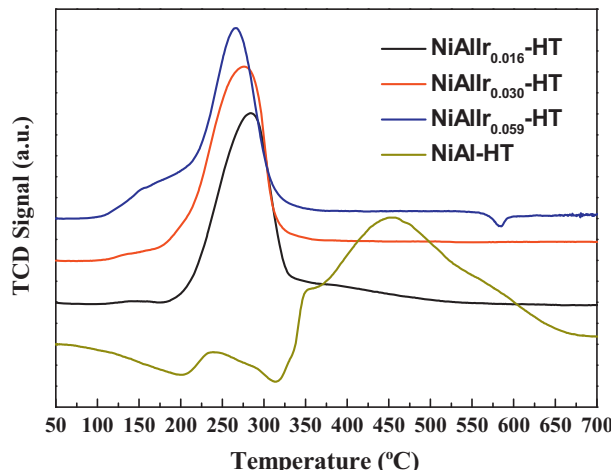


Fig. 3. H₂-TPR results of Ni–Al hydrotalcite (NiAl-HT) and after doping different amounts of Ir.

Ir contents presented similar average Ni particle size of ~3.0 nm, calculated by using Scherrer equation (Table 2). In contrast, the Ni particle size of the $\text{Ni}/\text{Al}_2\text{O}_3$ catalyst is ~4.0 nm. This smaller Ni particle size observed on $\text{NiIr}_x/\text{Al}_2\text{O}_3$ catalysts was due to the lower reduction temperature (300 °C) compared with that for $\text{Ni}/\text{Al}_2\text{O}_3$ (500 °C).

In order to make further investigation on the structure of $\text{NiIr}_x/\text{Al}_2\text{O}_3$ catalysts, X-ray absorption spectroscopy (XAS) experiments were carried out to provide information on the oxidation state and local structure of Ir. As shown in Fig. 5a, XANES spectra at Ir L₃-edge of $\text{NiIr}_x/\text{Al}_2\text{O}_3$ catalysts are compared with the standard Ir foil and commercial IrO_2 oxide, illustrating the chemical status of Ir in different catalysts. The results show that all spectra for $\text{NiIr}_x/\text{Al}_2\text{O}_3$ catalysts exhibit similar edge energy and peak intensity compared with that for Ir foil, suggesting that most of Ir species in the catalysts are fully reduced [24,25]. The extended-edge (EXAFS) part for different catalysts could give more specific information about the local surrounding structure of the center metal Ir. Fig. 5b shows the Fourier transform of Ir L₃-edge EXAFS oscillations for the corresponding samples. The k -range used in the transform was chosen in order to exclude the regions of noise at high- k [26]. Obviously, the distance between absorber and backscatter atoms for Ni–Ir bimetallic catalysts is quite different from the standard samples. The major peak for all the $\text{NiIr}_x/\text{Al}_2\text{O}_3$ catalysts (Peak 2) could be corresponded to the formation of Ir–Ni bond [27], which is shorter than that for Ir–Ir bond in Ir foil (Peak 3), but longer than Ir–O bond in standard IrO_2 oxide (Peak 1). This data is in line with the results obtained from XRD. The extended-edge data were further fitted to obtain details of the surrounded environment of Ir atoms (Table 4). For all the $\text{NiIr}_x/\text{Al}_2\text{O}_3$ catalysts, only Ni–Ir bond could be found, which confirms the formation of Ir–Ni alloy and also illustrates that all of the Ir atoms were isolated and surrounded by

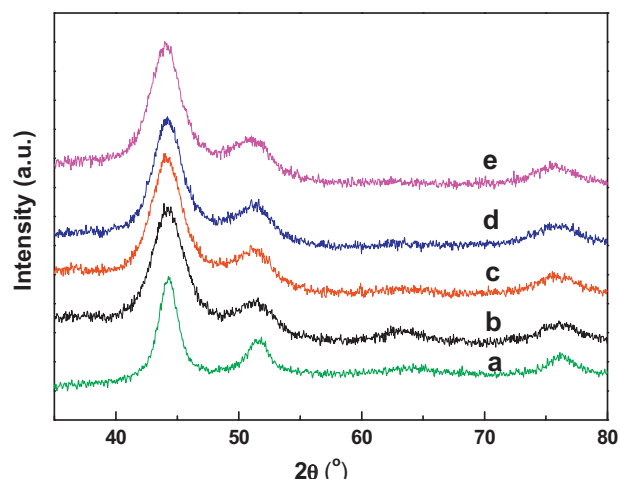


Fig. 4. XRD patterns of: (a) $\text{Ni}/\text{Al}_2\text{O}_3$; (b) $\text{NiIr}_{0.016}/\text{Al}_2\text{O}_3$; (c) $\text{NiIr}_{0.030}/\text{Al}_2\text{O}_3$; (d) $\text{NiIr}_{0.046}/\text{Al}_2\text{O}_3$; (e) $\text{NiIr}_{0.059}/\text{Al}_2\text{O}_3$. The samples were reduced at 300 °C before the test.

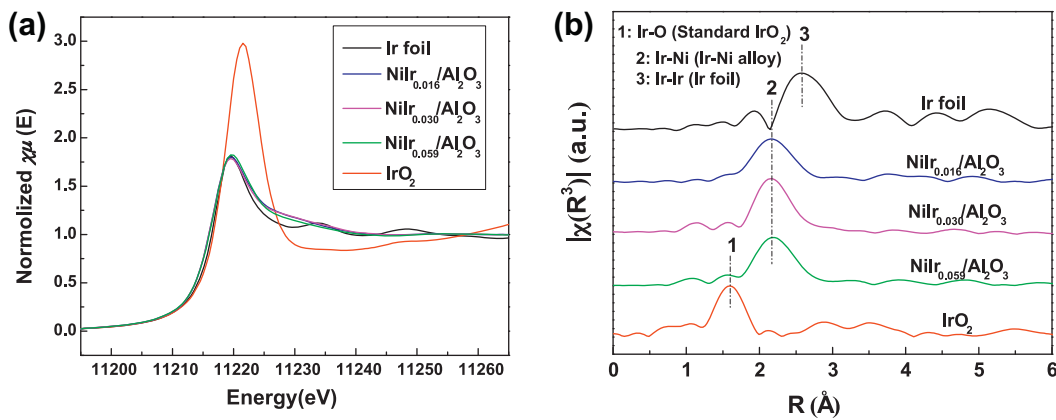


Fig. 5. The XAFS results for $\text{NiIr}_x/\text{Al}_2\text{O}_3$ catalysts: (a) the near-edge profiles; (b) the corresponding R -space profiles (without phase correction).

Table 4

Curve fitting results of Ir L₃-edge EXAFS of $\text{NiIr}_x/\text{Al}_2\text{O}_3$ catalysts.

Samples	Shell	CN ^a	R^b (Å)	R factor (%)	$\Delta\sigma^{2c}$ (10^{-3})	E_0^{d} (eV)
Ir foil	Ir–Ir	12	2.70	1.21	3.00	6.30
$\text{NiIr}_{0.016}/\text{Al}_2\text{O}_3$	Ir–Ni	9.4	2.53	1.12	9.28	5.78
$\text{NiIr}_{0.030}/\text{Al}_2\text{O}_3$	Ir–Ni	9.4	2.54	1.49	8.18	7.79
$\text{NiIr}_{0.059}/\text{Al}_2\text{O}_3$	Ir–Ni	7.6	2.53	0.31	6.15	6.87

^a Coordination number.

^b Distance between absorber and backscatter atoms.

^c Change in the Debye–Waller factor value relative to the Debye–Waller factor of the reference compound.

^d Inner potential correction to account for the difference in the inner potential between the sample and the reference compound.

Ni atoms. To be noted, the coordination number of Ni–Ir bond is 9.4 for either $\text{NiIr}_{0.016}/\text{Al}_2\text{O}_3$ or $\text{NiIr}_{0.030}/\text{Al}_2\text{O}_3$ catalysts, and 7.6 for $\text{NiIr}_{0.059}/\text{Al}_2\text{O}_3$ catalyst, all of which are lower than that for Ir foil ($CN=12$). The lower coordination number is due to the smaller particle size of Ir in the catalysts compared with its bulk sample. Moreover, the CN of Ir–Ni decreases with the increase of Ir contents because of the Ni–Ir alloy enrichment on the surface, which leads to more unsaturated Ir atoms.

3.1.3. H_2 adsorption property of $\text{NiIr}_x/\text{Al}_2\text{O}_3$ catalysts

The results presented above clearly confirm that Ni–Ir alloy was formed on $\text{NiIr}_x/\text{Al}_2\text{O}_3$ catalysts, which may further influence the adsorption property of the catalysts, and consequently play an important role for the promotion of catalytic performance. As H_2 is the target product for hydrous hydrazine decomposition, the change of H_2 adsorption on $\text{NiIr}_x/\text{Al}_2\text{O}_3$ catalysts was detected by microcalorimetric experiments. This measurement can provide not only the uptake of the probe molecules (e.g. H_2 , CO), but also the distribution of differential adsorption heat as a function of the coverage [28]. Fig. 6 displays the differential heat of H_2 adsorption at 40 °C as a function of H_2 uptake over $\text{Ni}/\text{Al}_2\text{O}_3$, $\text{NiIr}_{0.030}/\text{Al}_2\text{O}_3$, and $\text{NiIr}_{0.059}/\text{Al}_2\text{O}_3$ catalysts. The saturated amount of H_2 adsorption was 729 $\mu\text{mol g}^{-1}$ for $\text{Ni}/\text{Al}_2\text{O}_3$, which is much larger than those of $\text{NiIr}_{0.030}/\text{Al}_2\text{O}_3$ (680 $\mu\text{mol g}^{-1}$) and $\text{NiIr}_{0.059}/\text{Al}_2\text{O}_3$ (253 $\mu\text{mol g}^{-1}$). Simultaneously, the corresponding initial heats of H_2 chemisorption over these three catalysts were 87.0 kJ mol⁻¹, 76.8 kJ mol⁻¹, and 71.4 kJ mol⁻¹, respectively, indicating that the binding energy between H_2 and Ni could be greatly weakened by alloying Ni with Ir, similar to Pt-modified Ni catalyst [17]. This weakening phenomenon coincided well with the results over model catalysts [29–31]. As the bonding of H_2 was weaker on Ni–Ir alloy surface, the produced H_2 became easier to desorb from the catalyst. Consequently, the activity could be greatly improved over Ni–Ir alloy surface.

In spite of the low activity of Ni catalyst and the poor H_2 selectivity of Ir, alloying of Ni with Ir has led to improved catalytic

performance in terms of reactivity and H_2 selectivity. The alloying effect has been discussed on the grounds of two complementary effects: the geometric and the electronic [32–34]. Both appear to rationalize the catalytic ability of Ni–Ir alloy towards the selective decomposition of hydrous hydrazine. The alloying of Ni with Ir induced a change of the electronic properties of Ni, which influenced the chemisorption bond strength as evidenced by the H_2 microcalorimetric experiments. It has been reported that the preferred cleavage of N–H bond instead of N–N bond leads to the complete decomposition of $N_2\text{H}_4$ to N_2 and H_2 [35]. Therefore, the rupture of first N–H bond ($N_2\text{H}_4 \rightarrow N_2\text{H}_3^+ + \text{H}^+$) is thought to be crucial to produce hydrogen [10,36]. Chen and coworkers have shown that Ni–Pt-catalyzed NH_3 decomposition was facilitated due to the decreased energy barrier for N–H dissociation and destabilized surface intermediates NH_x [31]. Similarly, the formation of Ni–Ir alloy could make the cleavage of N–H bond much easier and also

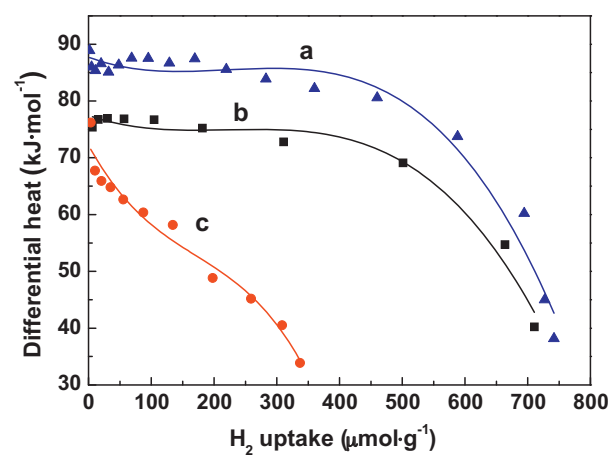


Fig. 6. Microcalorimetry results of H_2 adsorption on $\text{NiIr}_x/\text{Al}_2\text{O}_3$ catalysts: (a) $\text{Ni}/\text{Al}_2\text{O}_3$; (b) $\text{NiIr}_{0.030}/\text{Al}_2\text{O}_3$; (c) $\text{NiIr}_{0.059}/\text{Al}_2\text{O}_3$.

facilitate the desorption of the reaction intermediates [37], which is critical for the selective decomposition of hydrous hydrazine.

On the other hand, the H₂ selectivity over Ni/Al₂O₃ catalysts was increased from 93% to over 99% after addition of Ir. This is a surprisingly high selectivity because Ir nanoparticles by itself exhibited very high activity but poor H₂ selectivity. It appears that N₂H₄ decomposition on Ir was inhibited by alloying with Ni. To be noted, the EXAFS study puts in evidence the atomically dispersed Ir species in the host Ni nanoparticles. If we make the assumption that at least two neighboring surface Ir atoms were needed for N₂H₄ decomposition, we can interpret that isolated Ir atoms would play mainly a role in activating the Ni catalyst for selective decomposition of hydrous hydrazine. Results obtained recently on the Ir₁/Fe₂O₃ catalyst confirm this point. This atomically dispersed Ir catalyst did not exhibit any activity in hydrous hydrazine decomposition even at 50 °C (Fig. S2). Thus, the activity of Ir toward N₂H₄ decomposition was greatly changed by alloying with Ni, which was beneficial for H₂ selectivity in this case. These results of NiIr_x/Al₂O₃ catalysts also indicate the role of geometric effect.

The H₂ selectivity was 99% over NiIr_{0.059}/Al₂O₃, which is surprisingly high because Ir nanoparticle itself exhibited high activity for N₂H₄ decomposition to produce NH₃ instead of H₂ at low temperature [19]. It appears that this process was inhibited by alloying Ir with Ni. To be noted, the EXAFS study puts in evidence the atomically dispersed Ir species in the host Ni nanoparticles. If it is assumed that at least two neighboring surface Ir atoms were necessary for the first step of N₂H₄ activation, the isolated Ir atoms would be inert for decomposition of hydrous hydrazine. Results obtained recently on the Ir₁/Fe₂O₃ catalyst confirm this point. This atomically dispersed Ir catalyst did not exhibit any activity in hydrous hydrazine decomposition even at 50 °C (Fig. S2). Thus, the additional Ir atoms only played a role of modifying Ni instead of catalyzing the N₂H₄ decomposition to NH₃, which consequently promoted H₂ selectivity from 93% to over 99%. This promoting phenomenon also reflected the role of geometric effect for Ni–Ir alloy.

3.2. Structural configuration of NiIr_{0.059}/Al₂O₃ reduced at different temperatures

3.2.1. Hydrous hydrazine decomposition test

It has been reported that the catalytic performance was quite sensitive to the structural configuration of Ni-based bimetallic catalysts [23]. To further investigate the relationship between the structural change and the catalytic property of Ni–Ir catalyst, NiIr_{0.059}/Al₂O₃ catalyst was chose as a model. The catalytic performance to hydrous hydrazine decomposition was studied over NiIr_{0.059}/Al₂O₃ catalyst reduced in H₂ at various temperatures (Fig. 7). As mentioned above, the hydrogen selectivity was 99% with reaction rate of 12.4 h⁻¹ when the catalyst was reduced at 300 °C. However, the H₂ selectivity decreased to 88% with the reaction rate of 8.1 h⁻¹ if reduced at 500 °C and further decreased to 65% with reaction rate of 3.6 h⁻¹ if pretreated at 700 °C (Table 5). Obviously, the catalytic performance of Ni–Ir bimetallic catalyst in hydrous hydrazine decomposition was sensitive to the pretreatment temperature, as has been noted previously [27,38,39]. We firstly attributed this decrease in H₂ selectivity and activity to the Ni particle aggregation occurred during the high temperature treatment. However, the H₂ selectivity remained as high as 92% for monometallic Ni/Al₂O₃ catalyst if reduced at 800 °C (Table 5), which has the similar Ni particles size with the NiIr_{0.059}/Al₂O₃-700R. This interesting phenomenon intrigued us to clarify the detailed structure of NiIr_{0.059}/Al₂O₃ catalysts reduced at various temperatures.

3.2.2. Structural analysis of NiIr_{0.059}/Al₂O₃ catalysts

XRD measurements were carried out for the freshly reduced samples to investigate the primary structure of NiIr_{0.059}/Al₂O₃

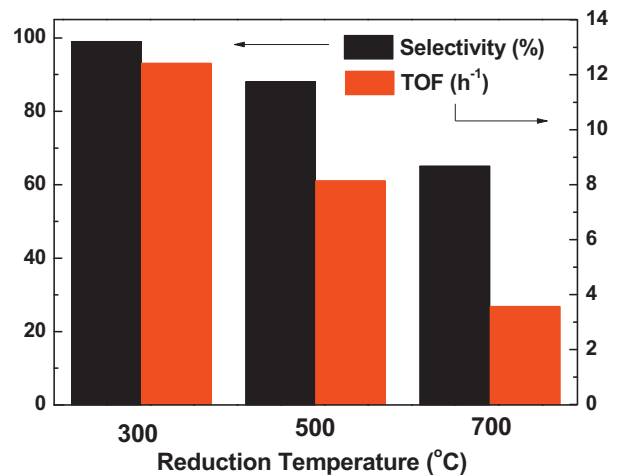


Fig. 7. The comparison of selectivity and reaction rate for hydrous hydrazine decomposition of NiIr_{0.059}/Al₂O₃ catalyst reduced at different temperatures. The reaction temperature was 30 °C.

catalyst (Fig. S3). For NiIr_{0.059}/Al₂O₃-500R and NiIr_{0.059}/Al₂O₃-700R, the main diffraction peaks were observed at 44.0°, 51.4°, and 75.9°, respectively. There is no shift of the three peaks compared with NiIr_{0.059}/Al₂O₃ catalyst reduced at 300 °C, which indicates that the primary composition of Ni–Ir alloy did not change with the reduction temperatures. However, the signal intensity was significantly enhanced with increasing reduction temperature from 300 °C to 700 °C, reflecting the growth of Ni particle size. Calculated by Scherrer equation, the Ni particle size grows from 3.0 nm to 8.2 nm. To investigate the size effect, monometallic Ni/Al₂O₃ catalyst was also pretreated at 500 °C and 800 °C different temperatures to obtain similar Ni particle size as that for NiIr_{0.059}/Al₂O₃ (Table 5). As a result, the growing of Ni particle size for Ni/Al₂O₃ was accompanied by a decrease of reaction rate from 2.2 h⁻¹ to 1.7 h⁻¹. However, the H₂ selectivity remained as high as 92%. It illustrates that larger particle size may decrease the reaction rate but has little influence on the selectivity to H₂. In this case, structural configuration modification, induced by high-temperature reduction, may be the main reason for H₂ selectivity decline.

Further investigation was carried out by XAS experiments to get information of the local surrounding structure of the Ir. Fig. 8a shows the near edge spectra of Ir L₃-edge in NiIr_{0.059}/Al₂O₃ catalyst reduced at different temperatures and the reference samples (Ir foil and IrO₂). For all the NiIr_{0.059}/Al₂O₃ catalysts, Ir species were considered to be fully reduced because the edge energy showed no shift and the peak intensities were quite similar to Ir foil. The corresponding extended edge results after Fourier transformation could give more information about the surrounding environment of Ir atoms (Fig. 8b). The distances between Ir and the first nearest neighboring atoms were the same for all the NiIr_{0.059}/Al₂O₃ catalysts (Peak 2), which represents the existence of Ir–Ni bond. The results illustrate that Ni–Ir alloy was formed for all the samples, which is in line with those obtained by XRD measurements (Fig. S3). Curve fittings were also carried out for detailed information, summarized in Table 6. Only Ir–Ni bond could be found in the fitting results. It elucidates that most Ir atoms were highly dispersed in the catalyst and surrounded by Ni atoms in the form of Ni–Ir alloy, even after reduction at high temperatures (700 °C). To be noted, the coordination number (CN) of Ir–Ni increased from 7.6 to 9.9 with increasing the reduction temperature from 300 °C to 700 °C. This CN growth of Ir–Ni was due to the aggregation of Ni particles, which induced the migration of Ir atoms into an inner part of the sample. It has been reported that high temperature reduction often induces the segregation of one kind of metal to the topmost

Table 5

Selectivity and reaction rate comparisons for $\text{NiPt}_{0.059}/\text{Al}_2\text{O}_3$ and $\text{Ni}/\text{Al}_2\text{O}_3$ catalysts reduced at different temperatures.

Catalysts	Reduction temperature ($^{\circ}\text{C}$)	Ni particle size (nm)	Selectivity x (%)	Reaction rate (h^{-1})
$\text{Nilr}_{0.059}/\text{Al}_2\text{O}_3$	300	3.0	99	12.4
	500	4.7	88	8.1
	700	8.2	65	3.6
$\text{Ni}/\text{Al}_2\text{O}_3$	500	4.0	93	2.2
	700	6.3	93	2.0
	800	8.7	92	1.7

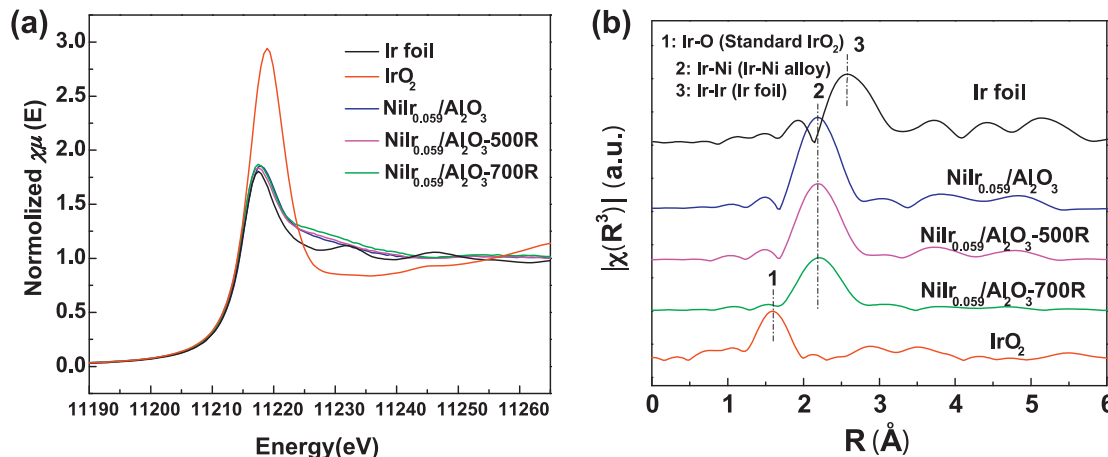


Fig. 8. The XAFS results for $\text{Nilr}_{0.059}/\text{Al}_2\text{O}_3$ catalysts reduced at different temperatures: (a) the near-edge profiles; (b) the corresponding R -space profiles (without phase correction).

surface [27,38–42]. As the surface energy for Ir is 3.000 J m^{-2} , much higher than Ni (2.450 J m^{-2}) [43], there is a trend for Ir atoms to locate inside of the Ni–Ir nanoparticles. In addition, the Ni particle size increased after high temperature reduction (700°C), which may also lead to the increase of Ir–Ni coordination number.

3.2.3. H_2 adsorption property of $\text{Nilr}_x/\text{Al}_2\text{O}_3$ catalysts

It has been discussed above that reduction at 700°C drives the diffusion of Ir atoms into the Ni bulk and produces a Ni-skin surface, which could be reflected by adsorption property change of $\text{Nilr}_{0.059}/\text{Al}_2\text{O}_3$ catalyst. Comparing the microcalorimetry results for H_2 adsorption over $\text{Nilr}_{0.059}/\text{Al}_2\text{O}_3$ catalyst reduced at 300°C , 500°C , and 700°C , the adsorption amount of H_2 were similar but the adsorption heat distributions were quite different from each other (Fig. 9). As increasing the reduction temperature, the H_2 adsorption heat also increases, and $\text{Nilr}_{0.059}/\text{Al}_2\text{O}_3-700\text{R}$ displays very similar adsorption energy as $\text{Ni}/\text{Al}_2\text{O}_3$. The observed increase of H_2 adsorption heat further confirms the Ni-skin structure of $\text{Nilr}_{0.059}/\text{Al}_2\text{O}_3$ catalyst after high-temperature reduction, e.g. 700°C .

It is interesting to note that the Ir atoms preferred to remain in the Ni bulk at high reduction temperatures. Consequently, when large amount of Ni–Ir alloy posited inside of the particle with a Ni-skin surface, the electronic environment of this surface may quite different from the Ni–Ir alloy surface. Therefore, the lost of catalytic activity and H_2 selectivity over $\text{Nilr}_{0.059}/\text{Al}_2\text{O}_3$ after 700°C reduction can be partly mainly attributed to the formed Ni-skin

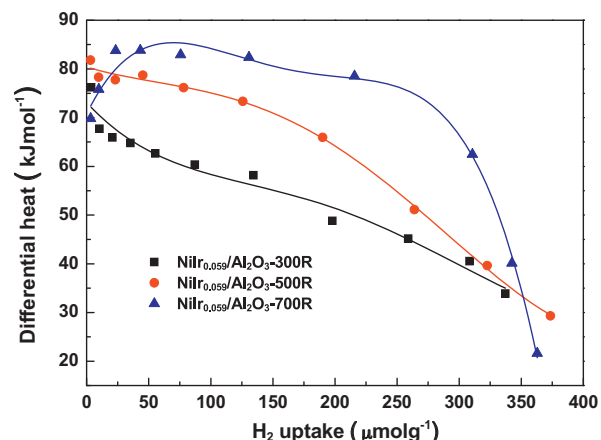


Fig. 9. Differential heats of H_2 adsorption at 40°C as a function of surface coverage on $\text{Nilr}_{0.059}/\text{Al}_2\text{O}_3$ catalyst reduced at different temperatures.

surface. Moreover, we cannot exclude the possibility that small amount of Ir is present outside the nanoparticles, which may lead to severe decline of H_2 selectivity. Actually, 0.10 wt% of Ir particle, if segregated on the surface, may induce a severe decline of the H_2 selectivity to 65% although they could not be detected by XRD or XAFS results [44]. Examination of the $\text{Nilr}_{0.059}/\text{Al}_2\text{O}_3-300\text{R}$ and $\text{Nilr}_{0.059}/\text{Al}_2\text{O}_3-700\text{R}$ samples by means of HAADF-STEM (Fig. S4) has demonstrated that a very small amount of Ir atoms indeed

Table 6

Curve fitting results of Ir L₃-edge EXAFS of $\text{Nilr}_{0.059}/\text{Al}_2\text{O}_3$ catalyst reduced at different temperatures.

Samples	Shell	CN	R (Å)	R factor (%)	$\Delta\sigma^2$ (10^{-3})	E_0 (eV)
Ir foil	Ir–Ir	12	2.70	1.21	3.00	6.30
$\text{Nilr}_{0.059}/\text{Al}_2\text{O}_3$	Ir–Ni	7.6	2.53	0.31	6.15	6.87
$\text{Nilr}_{0.059}/\text{Al}_2\text{O}_3-500\text{R}$	Ir–Ni	9.2	2.52	0.23	4.93	7.13
$\text{Nilr}_{0.059}/\text{Al}_2\text{O}_3-700\text{R}$	Ir–Ni	9.9	2.52	0.41	1.36	6.90

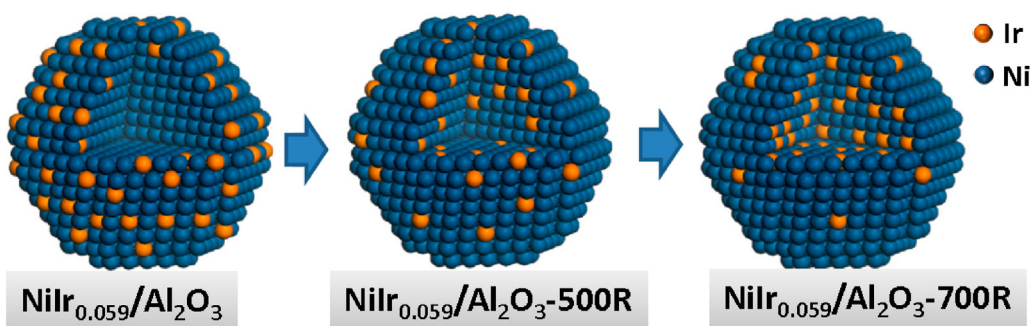


Fig. 10. Structure model of $\text{NiIr}_{0.059}/\text{Al}_2\text{O}_3$ catalyst reduced at different temperatures.

segregated on the surface after high temperature reduction, e.g. 700°C . Thus, this small amount of Ir particle may significantly reduce the H_2 selectivity, because the $\text{Ir}/\text{Al}_2\text{O}_3$ catalyst itself is highly active for this reaction with a poor selectivity (Table 2). As a result, high temperature reduction led to a severe decrease of H_2 selectivity for Ni–Ir catalyst. These observations were shown in the particle illustration at Fig. 10. Although XRD and XAFS results indicated that all the Ir atoms distributed in the bulk Ni to form Ni–Ir alloy, we cannot exclude the possibility that small amount of segregated Ir cluster is present outside the nanoparticles because the reduction temperature was 700°C . Actually, only about 0.1 wt% of Ir particle, if segregated on the surface, may induce a severe decline of the H_2 selectivity to 65%, which was calculated by assuming that Ir and Ni showed their own properties separately for this reaction. Although this trace amount of Ir species is out of the detection limit of XRD or XAFS [44], comparison of HAADF-STEM (Fig. S4) images of $\text{NiIr}_{0.059}/\text{Al}_2\text{O}_3$ -300R and $\text{NiIr}_{0.059}/\text{Al}_2\text{O}_3$ -700R samples demonstrated that a very small amount of Ir atoms indeed segregated on the surface after 700°C reduction. As a result, high temperature reduction led to diffusion of most of Ir atoms into the Ni particle and trace amount of Ir segregated on the surface at the same time. Both of the reasons led to severe decrease of H_2 selectivity. Based on the experimental results, the particle illustrations are shown in Fig. 10 to describe the structural change of Ni–Ir catalyst reduced at different temperatures.

3.3. Comparison of $\text{NiIr}_{0.030}/\text{Al}_2\text{O}_3$, $\text{NiPt}_{0.027}/\text{Al}_2\text{O}_3$, and $\text{NiAu}_{0.020}/\text{Al}_2\text{O}_3$ catalysts

3.3.1. Hydrous hydrazine decomposition test

We also compared the modification effect of different noble metals in bimetallic $\text{NiIr}_{0.030}/\text{Al}_2\text{O}_3$, $\text{NiPt}_{0.027}/\text{Al}_2\text{O}_3$, and $\text{NiAu}_{0.020}/\text{Al}_2\text{O}_3$ catalysts. Although Ir, Pt, and Au belong to the same period and the weight loadings are similar, the corresponding bimetallic catalysts exhibited quite different performances in hydrous hydrazine decomposition (Table 7). Compared with monometallic Ni catalyst, the selectivity increased from 93% to 99% and 97% with much higher reaction rate for Ir and Pt doped

Table 7
Hydrous hydrazine decomposition over monometallic and bimetallic catalysts.

Catalysts	Reaction rate (h^{-1})	Selectivity (%)
$\text{NiIr}_{0.030}/\text{Al}_2\text{O}_3$	8.0	99
$\text{NiPt}_{0.027}/\text{Al}_2\text{O}_3$	7.8	97
$\text{NiAu}_{0.020}/\text{Al}_2\text{O}_3$	2.0	81
$\text{Ni}/\text{Al}_2\text{O}_3$	2.2	93
$\text{Ir}/\text{Al}_2\text{O}_3$	788.0	6
$\text{Pt}/\text{Al}_2\text{O}_3$	–	–
$\text{Au}/\text{Al}_2\text{O}_3$	–	–

catalysts, respectively. On the contrary, the H_2 selectivity decreased to 81% with only 2.0 h^{-1} of reaction rate for $\text{NiAu}_{0.020}/\text{Al}_2\text{O}_3$ catalyst.

3.3.2. Structural analysis of $\text{NiNM}(\text{Ir}, \text{Pt}, \text{Au})_{x}/\text{Al}_2\text{O}_3$ catalysts

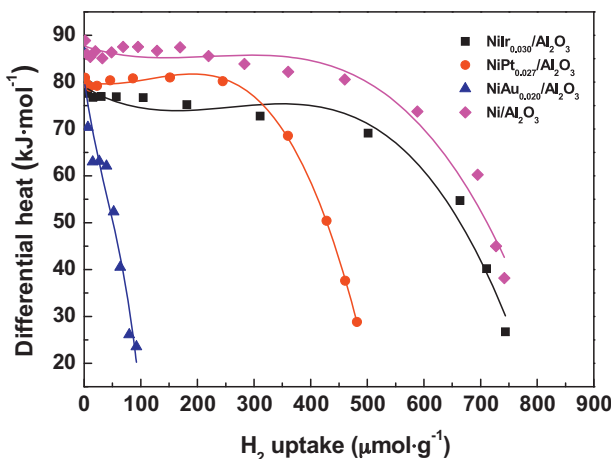
To clarify the structural difference of Ni–Ir, Ni–Pt and Ni–Au catalysts, we also did curve fittings for the three samples in XAFS experiments (Table 8). The total coordination numbers (CN) for the three samples are almost the same, which illustrates that the dispersion of different noble metals is quite similar on the surface of the catalysts. To be noted, there were only Ni–Ir bond found in the $\text{NiIr}_{0.030}/\text{Al}_2\text{O}_3$ catalyst, indicating a homogenous alloy of Ni–Ir in the sample. Tiny amount of Pt–Pt bond was observed in $\text{NiPt}_{0.027}/\text{Al}_2\text{O}_3$ catalyst. The CN for Pt–Pt bond was quite small with most of Pt atoms (88%) surrounded by Ni atoms. However, large amount of Au–Au bond were thought to be existed for $\text{NiAu}_{0.020}/\text{Al}_2\text{O}_3$ catalysts with only about 40% Au atoms coordinated with Ni. The alloy structure mainly depends on the difference of surface energy and atom radius between the two metals [45–47]. The radius of Au atom is 1.44 \AA , much larger than Ni atom (1.24 \AA). In comparison, the radii of Ir and Pt are 1.36 \AA and 1.39 \AA , respectively. Furthermore, the surface energy is 3.000 J m^{-2} for Ir and 2.475 J m^{-2} for Pt, which is similar to Ni (2.450 J m^{-2}). Therefore, it is comprehensible for the formation of homogeneous alloy of Ni–Ir and Ni–Pt. On the contrary, the surface energy is 1.520 J m^{-2} for Au, which is quite lower than Ni and may lead to easier aggregation of Au outside of Ni [40]. The different interaction between the noble metals and Ni could also be reflected by H_2 -TPR experiments (Fig. S5). Both Ir and Pt show a promotion effect for Ni reduction. There was only single H_2 consumption peak for each sample, which belongs to the co-reduction of Ni–Ir or Ni–Pt species. However, for $\text{NiAu}_{0.020}/\text{Al}_2\text{O}_3$ sample, the first narrow peak at 310°C belongs to the co-reduction of Ni–Au. The second broaden peak centered at 470°C could be associated to the reduction of highly dispersed Ni species, which are not intimately connected with Au [16].

3.3.3. H_2 adsorption property of $\text{NiNM}(\text{Ir}, \text{Pt}, \text{Au})_{x}/\text{Al}_2\text{O}_3$ catalysts

As mentioned above, large amount of Ni–Ir and Ni–Pt surface alloy are formed in $\text{NiIr}_{0.030}/\text{Al}_2\text{O}_3$ and $\text{NiPt}_{0.027}/\text{Al}_2\text{O}_3$ catalysts. The formation of alloy effectively altered the electronic properties of Ni and weakened the adsorption of H_2 , which could be confirmed by H_2 microcalorimetry results (Fig. 11). In contrast, for Ni–Au bimetallic catalyst, about 60% of Au atoms segregated on the surface. This segregation may lower the hydrogen production efficiency, because the $\text{Au}/\text{Al}_2\text{O}_3$ catalyst itself is inert for this reaction. Although H_2 adsorption over $\text{NiAu}_{0.020}/\text{Al}_2\text{O}_3$ catalyst was also weakened, this is most probably caused by the surface aggregated Au species because the H_2 chemisorption was very weak on Au nanoparticles [30].

Table 8Comparison of fitting results for different noble metal modified NiNM_x/Al₂O₃ catalysts.

Samples	Shell	CN	R (Å)	R factor (%)	$\Delta\sigma^2$ (10 ⁻³)	E ₀ (eV)	Structure model	
NiIr _{0.030} /Al ₂ O ₃	Ir–Ni	9.4	2.54	1.49	8.18	7.79		
NiPt _{0.027} /Al ₂ O ₃	Pt–Ni	8.3	2.54	0.50	2.9	6.90		
NiAu _{0.020} /Al ₂ O ₃	Pt–Pt Au–Ni	1.1 3.7	2.68 2.59	0.85	2.9 4.54	6.90 4.76		
	Au–Au	5.5	2.83			8.84	4.76	

**Fig. 11.** Microcalorimetry results for NiNM_x/Al₂O₃ catalysts (NM=Ir, Pt, Au) with similar noble metal amount.

4. Conclusion

Comparing with monometallic Ni/Al₂O₃ catalyst, NiIr_x/Al₂O₃ catalysts exhibited better selectivity and activity for hydrous hydrazine decomposition. Especially, the reaction rate increased to more than 6-fold with the Ir content of 0.059. The H₂ selectivity remained over 97% even after 10 times of usage and during the reaction temperature varied from 30 °C to 80 °C. The formation of Ni–Ir alloy was confirmed by means of XRD and XAFS characterizations. This Ni–Ir alloy may tune the interaction strength between N₂H₄ molecule and the catalyst, which made the N–H bond easier to break and also facilitated the desorption of reaction intermediates.

Compared with NiIr_{0.059}/Al₂O₃-300R, NiIr_{0.059}/Al₂O₃-700R exhibited only 65% of H₂ selectivity accompanied with a decrease of reaction rate to one-fourth. High temperature reduction led to the growth of Ni particles and drove the diffusion of Ir atoms in the Ni bulk. This Ni-skin surface altered the surface adsorption property of the catalyst and therefore was responsible for the decline of activity and selectivity.

Among the Ir, Pt, and Au doped Ni/Al₂O₃ catalysts, the CNs of Ir–Ni bond and Pt–Ni bond were larger than that observed for

Au–Ni, indicating that Ir and Pt were more easily alloyed with Ni than Au. The surface aggregation of Au over NiAu_{0.020}/Al₂O₃ may be the main reason of its lower activity and H₂ selectivity.

Acknowledgments

This work was supported by the National Natural Science Foundation of China (21103173, 21173218) and the “Hundred Talents Program of Dalian Institute of Chemical Physics”. We also acknowledge the Shanghai Synchrotron Radiation Facility (SSRF) and the National Synchrotron Radiation Research Center of Taiwan (NSRRC) for the XAS experiment.

Appendix A. Supplementary data

Supplementary data associated with this article can be found, in the online version, at <http://dx.doi.org/10.1016/j.apcatb.2013.10.022>.

References

- [1] J. Yang, A. Sudik, C. Wolverton, D.J. Siegel, Chem. Soc. Rev. 39 (2010) 656.
- [2] H.L. Jiang, S.K. Singh, J.M. Yan, X.B. Zhang, Q. Xu, ChemSusChem 3 (2010) 5412.
- [3] M. Yadav, Q. Xu, Energy Environ. Sci. 5 (2012) 9698.
- [4] E.W. Schmidt, Hydrazine and its Derivatives: Preparation, Properties, Applications, second ed., John Wiley & Sons, New York, 2001.
- [5] M. Zheng, R. Cheng, X. Chen, N. Li, L. Li, X. Wang, T. Zhang, Int. J. Hydrogen Energy 30 (2005) 1081.
- [6] S. Mary, C. Kappenstein, S. Balcon, S. Rossignol, E. Gengembre, Appl. Catal., A 182 (1999) 317.
- [7] S.K. Singh, Q. Xu, J. Am. Chem. Soc. 131 (2009) 18032.
- [8] S.K. Singh, Q. Xu, Chem. Commun. 46 (2010) 6545.
- [9] S.K. Singh, Q. Xu, Inorg. Chem. 49 (2010) 6148.
- [10] S.K. Singh, A.K. Singh, K. Aranishi, Q. Xu, J. Am. Chem. Soc. 133 (2011) 19638.
- [11] J. Song, R. Ran, Z. Shao, Int. J. Hydrogen Energy 35 (2010) 7919.
- [12] B. Zhao, J. Song, R. Ran, Z. Shao, Int. J. Hydrogen Energy 37 (2012) 1133.
- [13] J. Wang, X. Zhang, Z. Wang, L. Wang, Y. Zhang, Energy Environ. Sci. 5 (2012) 6885.
- [14] D.G. Tong, X.L. Zeng, W. Chu, D. Wang, P. Wu, Mater. Res. Bull. 45 (2010) 442.
- [15] D.G. Tong, W. Chu, P. Wu, G.F. Gu, L. Zhang, J. Mater. Chem. A 1 (2013) 358.
- [16] L. He, Y. Huang, A. Wang, X. Wang, X. Chen, J.J. Delgado, T. Zhang, Angew. Chem. Int. Ed. 51 (2012) 6191.
- [17] L. He, Y. Huang, A. Wang, Y. Liu, X. Liu, X. Chen, J.J. Delgado, X. Wang, T. Zhang, J. Catal. 298 (2013) 1.
- [18] D.G. Tong, D.M. Tang, W. Chu, G.F. Gu, P. Wu, J. Mater. Chem. A 1 (2013) 6425.
- [19] P. Zhang, Y. Wang, Y. Huang, T. Zhang, G. Wu, J. Li, Catal. Today 165 (2011) 80.
- [20] K. Takehira, J. Nat. Gas Chem. 18 (2009) 237.

- [21] B. Li, S. Kado, Y. Mukainakano, T. Miyazawa, T. Miyao, S. Naito, K. Okumura, K. Kunimori, K. Tomishige, *J. Catal.* 245 (2007) 144.
- [22] A. Tanksale, J.N. Beltramini, J.A. Dumesic, G.Q. Lu, *J. Catal.* 258 (2008) 366.
- [23] R. Ferrando, J. Jellinek, R.L. Johnston, *Chem. Rev.* 108 (2008) 845.
- [24] R.J. Trovitch, N. Guo, M.T. Janicke, H. Li, C.L. Marshall, J.T. Miller, A.P. Sattelberger, K.D. John, R.T. Baker, *Inorg. Chem.* 49 (2010) 2247.
- [25] A.M. Cruz, Ll. Abad, N.M. Carretero, J. Moral-Vico, J. Fraxedas, P. Lozano, G. Subías, V. Padial, M. Carballo, J.E. Collazos-Castro, N. Casan-Pastor, *J. Phys. Chem. C* 116 (2012) 5155.
- [26] R.B. Greengor, F.W. Lytle, *J. Catal.* 63 (1980) 476.
- [27] K. Sasaki, K.A. Kuttijiel, L. Barrio, D. Su, A.I. Frenkel, N. Marinkovic, D. Mahajan, R.R. Adzic, *J. Phys. Chem. C* 115 (2011) 9894.
- [28] R.D. Cortright, J.A. Dumesic, *J. Catal.* 148 (1994) 771.
- [29] J.R. Kitchin, N.A. Khan, M.A. Barteau, J.G. Chen, B. Yakshinskiy, T.E. Madey, *Surf. Sci.* 544 (2003) 295.
- [30] J. Greeley, M. Mavrikakis, *J. Phys. Chem. B* 109 (2005) 3460.
- [31] D.A. Hansgen, D.G. Blachos, J.G. Chen, *Nat. Chem.* 2 (2010) 484.
- [32] J.A. Rodriguez, D.W. Goodman, *Science* 257 (1992) 897.
- [33] J.R. Kitchin, J.K. Nørskov, M.A. Barteau, J.G. Chen, *Phys. Rev. Lett.* 93 (2004) 156801.
- [34] J. Greeley, M. Mavrikakis, *Nat. Mater.* 3 (2004) 810.
- [35] D.J. Alberas, J. Kiss, Z.M. Liu, J.M. White, *Surf. Sci.* 278 (1992) 51.
- [36] V. Rosca, M. Duca, M.T. Groot, M.T.M. Koper, *Chem. Rev.* 109 (2009) 2209.
- [37] R.T. Rewick, B.J. Wood, H. Wise, *J. Phys. Chem.* 19 (1979) 2480.
- [38] R. Mu, X. Guo, Q. Fu, X. Bao, *J. Phys. Chem. C* 115 (2011) 20590.
- [39] H. Xu, Q. Fu, Y. Yao, X. Bao, *Energy Environ. Sci.* 5 (2012) 6313.
- [40] R. Mu, Q. Fu, H. Xu, H. Zhang, Y. Huang, Z. Jiang, S. Zhang, D. Tan, X. Bao, *J. Am. Chem. Soc.* 133 (2011) 1978.
- [41] L.N. Akonwie, D.V. Kazachkin, D.R. Luebke, J.L. d'Itri, *Appl. Catal., A* 415–416 (2012) 59.
- [42] S.A. Tupy, A.M. Karim, C. Bagia, W. Deng, Y. Huang, D.G. Vlachos, J.G. Chen, *ACS Catal.* 2 (2012) 2290.
- [43] F.R. de Boer, R. Boom, W.C.M. Mattens, A.R. Miedema, A.K. Niessen, *Cohesion in Metals*, North-Holland, Amsterdam, 1989.
- [44] Y.W. Hsiao, Y. Tao, J.E. Shokes, R.A. Scott, U. Ryde, *Phys. Rev. B: Condens. Matter* 74 (2006) 214101.
- [45] A. Christensen, A.V. Ruban, P. Stoltze, K.W. Jacobsen, H.L. Skriver, J.K. Nørskov, *Phys. Rev. B* 56 (1997) 5822.
- [46] A.V. Ruban, H.L. Skriver, J.K. Nørskov, *Phys. Rev.* 59 (1999) 15990.
- [47] L. Wang, D.D. Johnson, *J. Am. Chem. Soc.* 131 (2009) 14023.